Acta Mech 234, 451–469 (2023)
https://doi.org/10.1007/s00707-022-03414-0

ORIGINAL PAPER

Pengfei Chai · Jianming Zhang · Rongxiong Xiao · Rui He · WeiCheng Lin

A multi-domain BEM based on the dual interpolation boundary face method for 3D potential problems

Received: 15 July 2022 / Revised: 19 October 2022 / Accepted: 20 October 2022 / Published online: 4 November 2022

Abstract In this paper, a multi-domain method, based on the dual interpolation boundary face method with Hermite-type moving-least-squares approximation (DiBFM-HMLS) and the matrix condensation technique, is firstly proposed for the 3D potential problems. This method is superior in the discontinuous field simulation (such as the corner problem) and can implement accurate interpolation in geometric structures with thin walls. Matrix condensation and reassembly reduce the overall system of linear algebraic equations to the interfacial ones with sparsity. This blocked-sparse-dominated multi-domain DiBFM-HMLS takes fewer CPU operations than its single-domain counterparts. Additionally, the interfacial conditions are not in the node-to-node format anymore, and instead, a node-to-element projective scheme built on the dual interpolation element of DiBFM-HMLS is presented for free mesh division in the interfaces (such as in self-adaption problems). Several numerical experiments from different aspects illustrate the feasibility and reliability of our multi-domain algorithms.

1 Introduction

The multi-domain boundary element method (MDBEM) has been added to various software packages for different functions [1, 2]. The basic idea of the multi-domain method is to decompose the entire domain into several homogeneous sub-regions, and connect subdomains by enforcing the equilibrium conditions and continuity conditions at the interface. The conventional MDBEM employ the band-shaped and sparse features of the overall coefficient matrix to improve the computational efficiency [3, 4]. Then, some researchers (Layton et al. [5], Kallivokas et al. [6], and Cheng et al. [7]) proposed ideas that utilized the advantage of the Galerkin method to construct a partial or complete symmetric form for the overall coefficient matrix to decrease the computation complexity. To pursue a fast solver, the multi-domain methods based on the linear least squares method [8] or the combination of GMRES and the fast multipole method (FMM) [9–11] were implemented to satisfy efficient solutions. Even for a large-scale potential problem with millions of degrees of freedom (DOFs), a microcomputer can obtain a reasonable solution using the MDBEM with FMM (Huang et al. [12]). Besides that, some pioneering works were presented to convert the scale of solution to the interface by the matrix condensation technique [13–16]; nonconforming elements were employed to avoid the discontinuous problem (e.g., tractions or flux) at the geometric corners. However, this leads to inaccurate interpolation at the geometric and physical corners, even the hyper-singular integral in the geometric models with thin walls.

The dual interpolation boundary face method with the moving least-squares approximation (DiBFM-MLS) [17–19] can simulate the discontinuous fields accurately by arranging two virtual points in the target places (see Fig. 1). The virtual points in DiBFM, not as collocation points in the boundary integral equation (BIE),

P. Chai · J. Zhang (✉) · R. Xiao · R. He · W. Lin
State Key Laboratory of Advanced Design and Manufacturing for Vehicle Body, College of Mechanical and Vehicle Engineering, Hunan University, Changsha 410082, China
e-mail: zhangjm@hnu.edu.cn

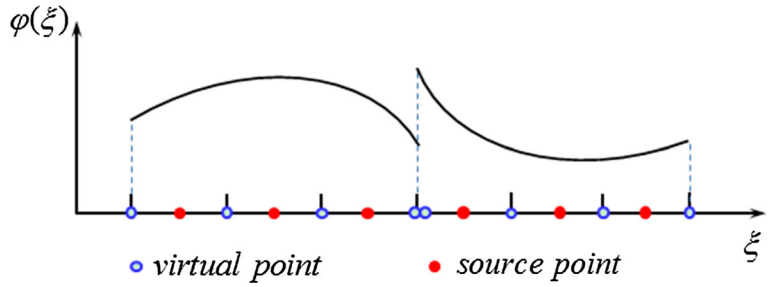

Fig. 1 Approximation of discontinuous field

are condensed by MLS approximation. Since the work was carried out on parametric coordinates, it will meet failure when constructing the MLS approximation for the virtual points on small feature sizes. Based on DiBFM-MLS, recently, our team proposed the dual interpolation boundary face method with Hermite-type moving-least-squares approximation (DiBFM-HMLS) [20, 21]. The normal equations are built on the Cartesian coordinate, and the influence domain is no longer limited to an edge. Thus DiBFM-HMLS possesses the advantage of dealing with structures with small feature sizes.

To use the properties of DiBFM-HMLS, we propose a multi-domain method, combining the matrix condensation technique and DiBFM-HMLS in this paper. Compared with its multi-domain counterpart, this method is more suitable for geometric structures with small feature sizes and can easily implement accurate interpolation in the geometric corner. Except for the discretization of the BIE, DiBFM-HMLS is also employed to supplement additional equations for interfacial virtual points. Moreover, this research replaced previous node-to-node interfacial conditions with the node-to-element ones building on the dual interpolation elements. This mapping scheme can provide convenience for free meshing in self-adaption problems. The coefficient matrix also presents the blocked-sparse and banded features, and following the increment in the number of subdomains, the sparsity is more significant, which can decrease the CPU time in the solution stage.

The paper is organized as follows: a brief introduction and the discretization form of the boundary integral equation (BIE) by DiBFM-HMLS for the potential problem are described in Sect. 2. The deduction of our multi-domain formulas for the 3D potential problem and the reassemble form is proposed in Sect. 3. Several numerical examples are contained in Sect. 4 to verify our multi-domain algorithm. Finally, Sect. 5 draws some conclusions and presents discussions for the addressed method in application and future work.

2 DiBFM-HMLS for 3D potential problems

2.1 Boundary integral equation for a single domain

Consider a 3D finite domain Ω enclosed by the boundary Γ ($\Gamma=\Gamma_B \cup \Gamma_I$, $\Gamma_B \cap \Gamma_I = \emptyset$). The governing differential equation with boundary and interface conditions for the potential problem is given by:

$$\begin{array}{ll} \nabla^2 u = 0, & \forall \mathbf{x} \in \Omega, \\ u = \bar{u}, & \forall \mathbf{x} \in \Gamma_d, \\ q = \frac{\partial u}{\partial n} = \bar{q}, & \forall \mathbf{x} \in \Gamma_n, \\ u_i = u_j,\ q_i = -q_j, & \forall \mathbf{x} \in \Gamma_I, \end{array} \tag{1}$$

where $\Gamma_B=\Gamma_d \cup \Gamma_n$ denotes the boundary and Γ_I is the interface in multi-domain problems between subdomain Ω_i and $\Omega_j (i \neq j)$. $\bar{u}$ and $\bar{q}$ are the prescribed values of the potential and the normal flux on the boundaries Γ_B, and n is the outward normal of the boundary Γ (see Fig. 2).

Through the employment of the Gauss formulas and divergence theorem, the governing differential equation can be written as boundary integral equation [22–24] (BIE):

$$c(P)u(P) = \int_\Gamma G^*(P,Q)q(Q)\mathrm{d}\Gamma(Q) - \int_\Gamma H^*(P,Q)u(Q)\mathrm{d}\Gamma(Q). \tag{2}$$

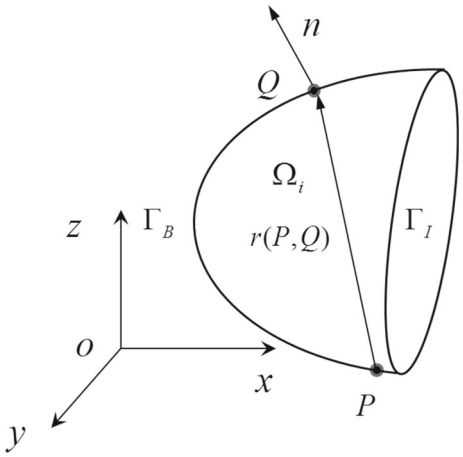

Fig. 2 A 3D finite domain Ω with interface

in Eq. (2), P represents the source point, Q denotes the field point, coefficient $c(P) = 1/2$ when P is located on the smooth surface, and $G^*(P,\ Q)$ and $H^*(P,\ Q)$ are fundamental solutions. For 3D potential problems, $G^*(P,\ Q)$ and $H^*(P,\ Q)$ are given by:

$$G^*(P, Q) = \frac{1}{4\pi}\frac{1}{r(P, Q)}, \tag{3}$$

$$H^*(P, Q) = \frac{\partial G^*(P, Q)}{\partial n(Q)} = -\frac{1}{4\pi r^2(P, Q)} r_{,k}(P, Q) n_{,k}(Q), \tag{4}$$

where $r(P,\ Q)$ is the distance between P and Q.

2.2 Discretization of the BIE

In this paper, the BIE is discretized by dual interpolation elements in DiBFM, where virtual points are not regarded as collation points. The discretization of Eq. (2) is given by

$$\sum_{l=1}^{\mathrm{NE}} \left(\sum_{\alpha=1}^{n\alpha} h_{ml}^{s_\alpha} u_l^{s_\alpha} + \sum_{\beta=1}^{n\beta} h_{ml}^{v_\beta} u_l^{v_\beta} \right) = \sum_{l=1}^{\mathrm{NE}} \left(\sum_{\alpha=1}^{n\alpha} g_{ml}^{s_\alpha} q_l^{s_\alpha} + \sum_{\alpha=1}^{n\beta} g_{ml}^{v_\beta} q_l^{v_\beta} \right), \quad m = 1, 2, ..., \mathrm{NS} \tag{5}$$

with

$$h_{ml}^{s_\alpha} = \int_{\Gamma_l} Q^*(P_m, Q) N_l^{s_\alpha}(Q) \mathrm{d}\Gamma(Q) + \frac{1}{2}\delta_{ml}^{s_\alpha}, \tag{6}$$

$$h_{ml}^{v_\beta} = \int_{\Gamma_l} Q^*(P_m, Q) N_l^{v_\beta}(Q) \mathrm{d}\Gamma(Q), \tag{7}$$

$$g_{ml}^{s_\alpha} = \int_{\Gamma_l} U^*(P_m, Q) N_l^{s_\alpha}(Q) \mathrm{d}\Gamma(Q), \tag{8}$$

$$g_{ml}^{v_\beta} = \int_{\Gamma_l} U^*(P_m, Q) N_l^{v_\beta}(Q) \mathrm{d}\Gamma(Q), \tag{9}$$

and

$$\delta_{ml}^{s_\alpha} = \begin{cases} 1, & \text{if the m}^{\text{th}}\text{source node is the } \alpha^{\text{th}} \text{ source node in the } l^{\text{th}} \text{ element,} \\ 0, \end{cases} \tag{10}$$

where NE, $n\alpha$, and $n\beta$ denote the numbers of elements, source nodes, and virtual nodes. $u_l^{s_\alpha}$, $q_l^{s_\alpha}$, $u_l^{v_\beta}$, and $q_l^{v_\beta}$ are the potential and normal flux of the αth source node and βth virtual node and on the lth element; $N_l^{s_\alpha}(Q)$

and $N_l^{v_\beta}(Q)$ represent the shape function of the source and virtual point, respectively. The matrix form of Eq. (5) is

$$\left[\mathbf{H}^{ss}\ \mathbf{H}^{sv}\right]\left\{\begin{array}{c}\mathbf{u}^s\\ \mathbf{u}^v\end{array}\right\}=\left[\mathbf{G}^{ss}\ \mathbf{G}^{sv}\right]\left\{\begin{array}{c}\mathbf{q}^s\\ \mathbf{q}^v\end{array}\right\} \tag{11}$$

where $\mathbf{u}^s$ and $\mathbf{q}^s$ (with NS × 1dimensional) are vectors of potential and normal flux for the source nodes, $\mathbf{u}^v$ and $\mathbf{q}^v$ (with NV × 1 dimensional) are vectors corresponding to the virtual nodes, and $\mathbf{H}^{ss}$(with NS × NS dimensional), $\mathbf{G}^{ss}$(with NS × NS dimensional), $\mathbf{H}^{sv}$(with NS × NV dimensional), and $\mathbf{G}^{sv}$(with NS × NV dimensional) (NS is the number of source points and NV is the number of virtual points) are coefficient matrices corresponding to $\mathbf{u}^s$, $\mathbf{q}^s$, $\mathbf{u}^v$, and $\mathbf{q}^v$.

2.3 Condensation of degrees of freedom for virtual nodes on the boundary

Decomposing the vectors $\mathbf{u}^v$ and $\mathbf{q}^v$ according to the boundary condition yields

$$\mathbf{u}^v=\overline{\mathbf{u}}^v_{\Gamma_B}+\hat{\mathbf{u}}^v_{\Gamma_B}+\hat{\mathbf{u}}^v_{\Gamma_I}, \tag{12}$$

$$\mathbf{q}^v=\overline{\mathbf{q}}^v_{\Gamma_B}+\hat{\mathbf{q}}^v_{\Gamma_B}+\hat{\mathbf{q}}^v_{\Gamma_I}, \tag{13}$$

where $\overline{\mathbf{u}}^v_{\Gamma_B}$, $\overline{\mathbf{q}}^v_{\Gamma_B}$(with NV × 1 dimensional) are known potential and normal fluxes of the virtual points on the boundary; $\hat{\mathbf{u}}^v_{\Gamma_B}$, $\hat{\mathbf{q}}^v_{\Gamma_B}$, and $\hat{\mathbf{u}}^v_{\Gamma_I}$, $\hat{\mathbf{q}}^v_{\Gamma_I}$(with NV × 1 dimensional) are unknown variables on the boundary and interface.

The unknown variables of $\hat{\mathbf{u}}^v_{\Gamma_B}$ and $\hat{\mathbf{q}}^v_{\Gamma_B}$ on the boundary can be condensed by HMLS [21], which can be expressed as

$$\hat{\mathbf{u}}^v_{\Gamma_B}=\boldsymbol{\Phi}^{vs}_{uu}\mathbf{u}^s+\boldsymbol{\Phi}^{vs}_{uq}\mathbf{q}^s, \tag{14}$$

$$\hat{\mathbf{q}}^v_{\Gamma_B}=\boldsymbol{\Phi}^{vs}_{qu}\mathbf{u}^s+\boldsymbol{\Phi}^{vs}_{qq}\mathbf{q}^s, \tag{15}$$

where $\boldsymbol{\Phi}^{vs}_{uu}$, $\boldsymbol{\Phi}^{vs}_{uq}$, $\boldsymbol{\Phi}^{vs}_{qu}$, and $\boldsymbol{\Phi}^{vs}_{qq}$ are the HMLS shape function matrices.

Through combination of Eqs. (11)–(15) and applying boundary conditions, the matrix form of Eq. (10) can be written as

$$\begin{aligned}&\left[\begin{array}{ccccc}\hat{\mathbf{M}}^{ss}_{\Gamma_B\Gamma_B}&\hat{\mathbf{H}}^{ss}_{\Gamma_B\Gamma_I}&\hat{\mathbf{H}}^{sv}_{\Gamma_B\Gamma_I}&-\hat{\mathbf{G}}^{ss}_{\Gamma_B\Gamma_I}&-\hat{\mathbf{G}}^{sv}_{\Gamma_B\Gamma_I}\\ \hat{\mathbf{M}}^{ss}_{\Gamma_I\Gamma_B}&\hat{\mathbf{H}}^{ss}_{\Gamma_I\Gamma_I}&\hat{\mathbf{H}}^{ss}_{\Gamma_I\Gamma_I}&-\hat{\mathbf{G}}^{ss}_{\Gamma_I\Gamma_I}&-\hat{\mathbf{G}}^{sv}_{\Gamma_I\Gamma_I}\end{array}\right]\left\{\begin{array}{c}\hat{\mathbf{x}}^s_{\Gamma_B}\\ \hat{\mathbf{u}}^s_{\Gamma_I}\\ \hat{\mathbf{u}}^v_{\Gamma_I}\\ \hat{\mathbf{q}}^s_{\Gamma_I}\\ \hat{\mathbf{q}}^v_{\Gamma_I}\end{array}\right\}\\ &=\left[\begin{array}{ccc}\overline{\mathbf{M}}^{ss}_{\Gamma_B\Gamma_B}&-\overline{\mathbf{H}}^{sv}_{\Gamma_B\Gamma_B}&\overline{\mathbf{G}}^{sv}_{\Gamma_B\Gamma_B}\\ \overline{\mathbf{M}}^{ss}_{\Gamma_I\Gamma_B}&-\overline{\mathbf{H}}^{sv}_{\Gamma_I\Gamma_B}&\overline{\mathbf{G}}^{sv}_{\Gamma_I\Gamma_B}\end{array}\right]\left\{\begin{array}{c}\overline{\mathbf{x}}^s_{\Gamma_B}\\ \overline{\mathbf{u}}^v_{\Gamma_B}\\ \overline{\mathbf{q}}^v_{\Gamma_B}\end{array}\right\}.\end{aligned} \tag{16}$$

For Dirichlet boundary condition:

$$\begin{aligned}\hat{\mathbf{M}}^{ss}_{\Gamma_B\Gamma_B}&=-\hat{\mathbf{G}}^{ss}_{\Gamma_B\Gamma_B},\ \ \hat{\mathbf{M}}^{ss}_{\Gamma_I\Gamma_B}=-\hat{\mathbf{G}}^{ss}_{\Gamma_I\Gamma_B},\\ \overline{\mathbf{M}}^{ss}_{\Gamma_I\Gamma_B}&=-\overline{\mathbf{G}}^{ss}_{\Gamma_B\Gamma_B},\ \ \overline{\mathbf{M}}^{ss}_{\Gamma_I\Gamma_B}=-\overline{\mathbf{G}}^{ss}_{\Gamma_I\Gamma_B},\end{aligned} \tag{17}$$

$$\overline{\mathbf{M}}^{ss}=\mathbf{H}^{ss}+\mathbf{H}^{sv}\boldsymbol{\Phi}^{vs}_{uu}-\mathbf{G}^{sv}\boldsymbol{\Phi}^{vs}_{qu}. \tag{18}$$

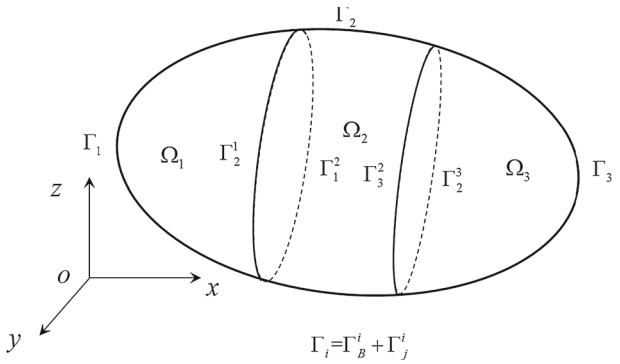

Fig. 3. 3D Multi-domain model for the potential problem

Neumann boundary condition:

$$\begin{aligned} \hat{\mathbf{M}}^{ss}_{\Gamma_B\Gamma_B} &= \hat{\mathbf{H}}^{ss}_{\Gamma_B\Gamma_B}, \quad \hat{\mathbf{M}}^{ss}_{\Gamma_I\Gamma_B} = \hat{\mathbf{H}}^{ss}_{\Gamma_I\Gamma_B}, \\ \overline{\mathbf{M}}^{ss}_{\Gamma_I\Gamma_B} &= \overline{\mathbf{G}}^{ss}_{\Gamma_B\Gamma_B}, \quad \overline{\mathbf{M}}^{ss}_{\Gamma_I\Gamma_B} = \overline{\mathbf{G}}^{ss}_{\Gamma_I\Gamma_B}, \end{aligned} \tag{19}$$

$$\overline{\mathbf{M}}^{ss} = \mathbf{G}^{ss} + \mathbf{G}^{sv}\boldsymbol{\Phi}^{vs}_{qq} - \mathbf{H}^{sv}\boldsymbol{\Phi}^{vs}_{uq}, \tag{20}$$

where $\overline{\mathbf{x}}^{s}_{\Gamma_B}$, $\overline{\mathbf{u}}^{v}_{\Gamma_B}$, and $\overline{\mathbf{q}}^{v}_{\Gamma_B}$ are the known vectors corresponding to the source and virtual nodes on the boundary; while $\hat{\mathbf{x}}^{s}_{\Gamma_B}$, and $\hat{\mathbf{u}}^{s}_{\Gamma_I}$, $\hat{\mathbf{q}}^{s}_{\Gamma_I}$, $\hat{\mathbf{u}}^{v}_{\Gamma_I}$, $\hat{\mathbf{q}}^{v}_{\Gamma_I}$ are the unknown variables on the boundary and interface, and $\overline{\mathbf{H}}^{ss}$, $\overline{\mathbf{G}}^{ss}$, $\hat{\mathbf{H}}^{ss}$, and $\hat{\mathbf{G}}^{ss}$ are the coefficient matrices corresponding to the known and unknown variables.

3 Multi-domain method based on DiBFM-HMLS

Consider a bounded Lipschitz domain Ω with boundary $\Gamma=\partial\Omega$. Let the domain be decomposed into M non-overlapping subdomains $\Omega_i (i = 1,2\ldots\mathrm{M}$, see Fig. 3), and the boundary is torn into several pieces Γ_i. Assuming that the skeleton Γ_i is surrounded by the boundary Γ^i_B and interface $\Gamma^i_j (i \neq j)$, respectively, where

$$\Omega = \bigcup_{i=1}^{\mathrm{M}} \Omega_i, \quad \Omega_i \cap \Omega_j = \emptyset, \ i \neq j,$$

$$\Gamma_i = \Gamma^i_B \cup \bigcup_{i=1}^{\mathrm{M}} \Gamma^i_j, \quad \Gamma^i_j = \Gamma_i \cap \Gamma_j, \ i \neq j.$$

Ω_j (j=1, 2, $\cdots$, M and $j \neq i$) is the subdomain contacting with Ω_i.

3.1 Condensation of variables on the boundary

The matrix form of BIE for a single domain with interfaces has been listed in Eq. (16). Since the virtual points are not regarded as collocation points in BIE, additional constraints are needed for the existing virtual points on the interface. This research introduces the HMLS approximation (see Eqs. (21), (22)) as the auxiliary equations for interfacial virtual points:

$$\hat{\mathbf{u}}^{v}_{\Gamma^i_j} = \boldsymbol{\Phi}^{uu}_{\Gamma^i_j\Gamma^i_B}\mathbf{u}^{s}_{\Gamma^i_B} + \boldsymbol{\Phi}^{uu}_{\Gamma^i_j\Gamma^i_j}\mathbf{u}^{s}_{\Gamma^i_j} + \boldsymbol{\Phi}^{uq}_{\Gamma^i_j\Gamma^i_B}\mathbf{q}^{s}_{\Gamma^i_B} + \boldsymbol{\Phi}^{uq}_{\Gamma^i_j\Gamma^i_j}\mathbf{q}^{s}_{\Gamma^i_j}, \tag{21}$$

$$\hat{\mathbf{q}}^{v}_{\Gamma^i_j} = \boldsymbol{\Phi}^{qu}_{\Gamma^i_j\Gamma^i_B}\mathbf{u}^{s}_{\Gamma^i_B} + \boldsymbol{\Phi}^{qu}_{\Gamma^i_j\Gamma^i_j}\mathbf{u}^{s}_{\Gamma^i_j} + \boldsymbol{\Phi}^{qq}_{\Gamma^i_j\Gamma^i_B}\mathbf{q}^{s}_{\Gamma^i_B} + \boldsymbol{\Phi}^{qq}_{\Gamma^i_j\Gamma^i_j}\mathbf{q}^{s}_{\Gamma^i_j}. \tag{22}$$

Through the combination of Eqs. (21) and 22), Eq. (16) can be rewritten as

$$\begin{bmatrix} \hat{\mathbf{M}}^{ss}_{\Gamma_B^i\Gamma_B^i} & \hat{\mathbf{H}}^{ss}_{\Gamma_B^i\Gamma_j^i} & \hat{\mathbf{H}}^{sv}_{\Gamma_B^i\Gamma_j^i} & -\hat{\mathbf{G}}^{ss}_{\Gamma_B^i\Gamma_j^i} & -\hat{\mathbf{G}}^{sv}_{\Gamma_B^i\Gamma_j^i} \\ \hat{\mathbf{M}}^{ss}_{\Gamma_j^i\Gamma_B^i} & \hat{\mathbf{H}}^{ss}_{\Gamma_j^i\Gamma_j^i} & \hat{\mathbf{H}}^{sv}_{\Gamma_j^i\Gamma_j^i} & -\hat{\mathbf{G}}^{ss}_{\Gamma_j^i\Gamma_j^i} & -\hat{\mathbf{G}}^{sv}_{\Gamma_j^i\Gamma_j^i} \\ \hat{\mathbf{\Theta}}^{vs}_{\Gamma_j^i\Gamma_B^i} & -\hat{\mathbf{\Phi}}^{vs}_{\Gamma_j^i\Gamma_j^i} & \mathbf{I} & -\hat{\mathbf{\Psi}}^{vs}_{\Gamma_j^i\Gamma_j^i} & -\mathbf{I} \end{bmatrix} \begin{Bmatrix} \hat{\mathbf{x}}^{s}_{\Gamma_B^i} \\ \hat{\mathbf{u}}^{s}_{\Gamma_j^i} \\ \hat{\mathbf{u}}^{v}_{\Gamma_j^i} \\ \hat{\mathbf{q}}^{s}_{\Gamma_j^i} \\ \hat{\mathbf{q}}^{v}_{\Gamma_j^i} \end{Bmatrix}$$
$$= \begin{bmatrix} \hat{\mathbf{M}}^{ss}_{\Gamma_B^i\Gamma_B^i} & -\overline{\mathbf{H}}^{sv}_{\Gamma_j^i\Gamma_B^i} & \overline{\mathbf{G}}^{sv}_{\Gamma_j^i\Gamma_B^i} \\ \hat{\mathbf{M}}^{ss}_{\Gamma_j^i\Gamma_B^i} & -\overline{\mathbf{H}}^{sv}_{\Gamma_j^i\Gamma_B^i} & \overline{\mathbf{G}}^{sv}_{\Gamma_j^i\Gamma_B^i} \\ \overline{\mathbf{\Theta}}^{vs}_{\Gamma_j^i\Gamma_B^i} & \mathbf{0} & \mathbf{0} \end{bmatrix} \begin{Bmatrix} \hat{\mathbf{x}}^{s}_{\Gamma_B^i} \\ \overline{\mathbf{u}}^{v}_{\Gamma_B^i} \\ \overline{\mathbf{q}}^{v}_{\Gamma_B^i} \end{Bmatrix} \tag{23}$$

For the Dirichlet boundary condition part:

$$\hat{\mathbf{\Theta}}^{vs}_{\Gamma_j^i\Gamma_B^i} = \hat{\mathbf{\Phi}}^{uu}_{\Gamma_j^i\Gamma_B^i} - \hat{\mathbf{\Phi}}^{qu}_{\Gamma_j^i\Gamma_B^i}, \quad \overline{\mathbf{\Theta}}^{vs}_{\Gamma_j^i\Gamma_B^i} = \overline{\mathbf{\Phi}}^{uu}_{\Gamma_j^i\Gamma_B^i} - \overline{\mathbf{\Phi}}^{qu}_{\Gamma_j^i\Gamma_B^i}, \tag{24}$$

and the Neumann boundary condition part:

$$\hat{\mathbf{\Theta}}^{vs}_{\Gamma_j^i\Gamma_B^i} = \hat{\mathbf{\Phi}}^{uq}_{\Gamma_j^i\Gamma_B^i} - \hat{\mathbf{\Phi}}^{qq}_{\Gamma_j^i\Gamma_B^i}, \quad \overline{\mathbf{\Theta}}^{vs}_{\Gamma_j^i\Gamma_B^i} = \overline{\mathbf{\Phi}}^{uq}_{\Gamma_j^i\Gamma_B^i} - \overline{\mathbf{\Phi}}^{qq}_{\Gamma_j^i\Gamma_B^i}, \tag{25}$$

where

$$\hat{\mathbf{\Psi}}^{vs}_{\Gamma_j^i\Gamma_j^i} = \hat{\mathbf{\Phi}}^{uq}_{\Gamma_j^i\Gamma_j^i} - \hat{\mathbf{\Phi}}^{qq}_{\Gamma_j^i\Gamma_j^i}, \tag{26}$$

$$\hat{\mathbf{\Phi}}^{vs}_{\Gamma_j^i\Gamma_j^i} = \hat{\mathbf{\Phi}}^{uu}_{\Gamma_j^i\Gamma_j^i} - \hat{\mathbf{\Phi}}^{qu}_{\Gamma_j^i\Gamma_j^i}. \tag{27}$$

A compact form of Eq. (23) is given by

$$\begin{bmatrix} \mathbf{BB}^{ss}_{\Gamma_B^i\Gamma_B^i} & \mathbf{BI}^{u_{ss}}_{\Gamma_B^i\Gamma_j^i} & \mathbf{BI}^{u_{sv}}_{\Gamma_B^i\Gamma_j^i} & -\mathbf{BI}^{q_{ss}}_{\Gamma_B^i\Gamma_j^i} & -\mathbf{BI}^{q_{sv}}_{\Gamma_B^i\Gamma_j^i} \\ \mathbf{IB}^{ss}_{\Gamma_j^i\Gamma_B^i} & \mathbf{II}^{u_{ss}}_{\Gamma_j^i\Gamma_j^i} & \mathbf{II}^{u_{sv}}_{\Gamma_j^i\Gamma_j^i} & -\mathbf{II}^{q_{ss}}_{\Gamma_j^i\Gamma_j^i} & -\mathbf{II}^{q_{sv}}_{\Gamma_j^i\Gamma_j^i} \\ \mathbf{IB}^{vs}_{\Gamma_j^i\Gamma_B^i} & \mathbf{II}^{u_{vs}}_{\Gamma_j^i\Gamma_j^i} & \mathbf{II}^{u_{vv}}_{\Gamma_j^i\Gamma_j^i} & -\mathbf{II}^{q_{vs}}_{\Gamma_j^i\Gamma_j^i} & -\mathbf{II}^{q_{vv}}_{\Gamma_j^i\Gamma_j^i} \end{bmatrix} \begin{Bmatrix} \mathbf{x}_{\Gamma_B^i} \\ \hat{\mathbf{u}}^{s}_{\Gamma_j^i} \\ \hat{\mathbf{u}}^{v}_{\Gamma_j^i} \\ \hat{\mathbf{q}}^{s}_{\Gamma_j^i} \\ \hat{\mathbf{q}}^{v}_{\Gamma_j^i} \end{Bmatrix} = \begin{Bmatrix} \mathbf{b}_{\Gamma_B^i} \\ \mathbf{b}_{\Gamma_j^i} \\ \mathbf{d}_{\Gamma_j^i} \end{Bmatrix} \tag{28}$$

in which **BB**, **BI**, **IB**, and **II** represent the boundary-boundary, boundary-interface, interface-boundary and interface-interface parts. In the block matrix **II**, entry **I** denotes the identity matrix.

By eliminating the degrees of freedom on the boundary, a system of linear equations concerning unknown interface variables can be given as

$$\begin{bmatrix} \mathbf{A}^{u_{ss}}_{\Gamma_j^i\Gamma_j^i} & \mathbf{A}^{u_{sv}}_{\Gamma_j^i\Gamma_j^i} \\ \mathbf{A}^{u_{vs}}_{\Gamma_j^i\Gamma_j^i} & \mathbf{A}^{u_{vv}}_{\Gamma_j^i\Gamma_j^i} \end{bmatrix} \begin{Bmatrix} \hat{\mathbf{u}}^{s}_{\Gamma_j^i} \\ \hat{\mathbf{u}}^{v}_{\Gamma_j^i} \end{Bmatrix} - \begin{bmatrix} \mathbf{A}^{q_{ss}}_{\Gamma_j^i\Gamma_j^i} & \mathbf{A}^{q_{sv}}_{\Gamma_j^i\Gamma_j^i} \\ \mathbf{A}^{q_{vs}}_{\Gamma_j^i\Gamma_j^i} & \mathbf{A}^{q_{vv}}_{\Gamma_j^i\Gamma_j^i} \end{bmatrix} \begin{Bmatrix} \hat{\mathbf{q}}^{s}_{\Gamma_j^i} \\ \hat{\mathbf{q}}^{v}_{\Gamma_j^i} \end{Bmatrix} = \begin{Bmatrix} \overline{\mathbf{b}}_{\Gamma_j^i} \\ \overline{\mathbf{d}}_{\Gamma_j^i} \end{Bmatrix}, \tag{29}$$

where

$$\begin{bmatrix} \mathbf{A}^{u_{ss}}_{\Gamma^i_j\Gamma^i_j} & \mathbf{A}^{u_{sv}}_{\Gamma^i_j\Gamma^i_j} \\ \mathbf{A}^{u_{vs}}_{\Gamma^i_j\Gamma^i_j} & \mathbf{A}^{u_{vv}}_{\Gamma^i_j\Gamma^i_j} \end{bmatrix} = \begin{bmatrix} \mathbf{II}^{u_{ss}}_{\Gamma^i_j\Gamma^i_j} & \mathbf{II}^{u_{sv}}_{\Gamma^i_j\Gamma^i_j} \\ \mathbf{II}^{u_{vs}}_{\Gamma^i_j\Gamma^i_j} & \mathbf{II}^{u_{vv}}_{\Gamma^i_j\Gamma^i_j} \end{bmatrix} - \begin{bmatrix} \mathbf{IB}^{ss}_{\Gamma^i_j\Gamma^i_B} \\ \mathbf{IB}^{vs}_{\Gamma^i_j\Gamma^i_B} \end{bmatrix} (\mathbf{BB}^{ss}_{\Gamma^i_B\Gamma^i_B})^{-1} \begin{bmatrix} \mathbf{BI}^{u_{ss}}_{\Gamma^i_B\Gamma^i_j} & \mathbf{BI}^{u_{sv}}_{\Gamma^i_B\Gamma^i_j} \end{bmatrix}, \tag{30}$$

$$\begin{bmatrix} \mathbf{A}^{q_{ss}}_{\Gamma^i_j\Gamma^i_j} & \mathbf{A}^{q_{sv}}_{\Gamma^i_j\Gamma^i_j} \\ \mathbf{A}^{q_{vs}}_{\Gamma^i_j\Gamma^i_j} & \mathbf{A}^{q_{vv}}_{\Gamma^i_j\Gamma^i_j} \end{bmatrix} = \begin{bmatrix} \mathbf{II}^{q_{ss}}_{\Gamma^i_j\Gamma^i_j} & \mathbf{II}^{q_{sv}}_{\Gamma^i_j\Gamma^i_j} \\ \mathbf{II}^{q_{vs}}_{\Gamma^i_j\Gamma^i_j} & \mathbf{II}^{q_{vv}}_{\Gamma^i_j\Gamma^i_j} \end{bmatrix} - \begin{bmatrix} \mathbf{IB}^{ss}_{\Gamma^i_j\Gamma^i_B} \\ \mathbf{IB}^{vs}_{\Gamma^i_j\Gamma^i_B} \end{bmatrix} (\mathbf{BB}^{ss}_{\Gamma^i_B\Gamma^i_B})^{-1} \begin{bmatrix} \mathbf{BI}^{q_{ss}}_{\Gamma_B\Gamma^i_j} & \mathbf{BI}^{q_{sv}}_{\Gamma^i_B\Gamma^i_j} \end{bmatrix}, \tag{31}$$

$$\begin{Bmatrix} \overline{\mathbf{b}}_{\Gamma^i_j} \\ \overline{\mathbf{d}}_{\Gamma^i_j} \end{Bmatrix} = \begin{Bmatrix} \mathbf{b}_{\Gamma^i_j} \\ \mathbf{d}_{\Gamma^i_j} \end{Bmatrix} - \begin{bmatrix} \mathbf{IB}^{ss}_{\Gamma^i_j\Gamma^i_B} \\ \mathbf{IB}^{vs}_{\Gamma^i_j\Gamma^i_B} \end{bmatrix} (\mathbf{BB}^{ss}_{\Gamma^i_B\Gamma^i_B})^{-1} \mathbf{b}_{\Gamma^i_B}. \tag{32}$$

Multiplying the left hand side of Eq. (29) by the inverse of $\begin{bmatrix} \mathbf{A}^{q_{ss}}_{\Gamma^i_j\Gamma^i_j} & \mathbf{A}^{q_{sv}}_{\Gamma^i_j\Gamma^i_j} \\ \mathbf{A}^{q_{vs}}_{\Gamma^i_j\Gamma^i_j} & \mathbf{A}^{q_{vv}}_{\Gamma^i_j\Gamma^i_j} \end{bmatrix}$, we can get

$$\begin{bmatrix} \widehat{A}^{u_{ss}}_{\Gamma^i_j\Gamma^i_j} & \widehat{A}^{u_{sv}}_{\Gamma^i_j\Gamma^i_j} \\ \widehat{A}^{u_{vs}}_{\Gamma^i_j\Gamma^i_j} & \widehat{A}^{u_{vv}}_{\Gamma^i_j\Gamma^i_j} \end{bmatrix} \begin{Bmatrix} \hat{\mathbf{u}}^s_{\Gamma^i_j} \\ \hat{\mathbf{u}}^v_{\Gamma^i_j} \end{Bmatrix} - \begin{Bmatrix} \hat{\mathbf{q}}^s_{\Gamma^i_j} \\ \hat{\mathbf{q}}^v_{\Gamma^i_j} \end{Bmatrix} = \begin{Bmatrix} \widehat{b}_{\Gamma^i_j} \\ \widehat{d}_{\Gamma^i_j} \end{Bmatrix}, \tag{33}$$

where

$$\begin{aligned} \begin{bmatrix} \widehat{A}^{u_{ss}}_{\Gamma^i_j\Gamma^i_j} & \widehat{A}^{u_{sv}}_{\Gamma^i_j\Gamma^i_j} \\ \widehat{A}^{u_{vs}}_{\Gamma^i_j\Gamma^i_j} & \widehat{A}^{u_{vv}}_{\Gamma^i_j\Gamma^i_j} \end{bmatrix} &= \begin{bmatrix} \mathbf{A}^{q_{ss}}_{\Gamma^i_j\Gamma^i_j} & \mathbf{A}^{q_{sv}}_{\Gamma^i_j\Gamma^i_j} \\ \mathbf{A}^{q_{vs}}_{\Gamma^i_j\Gamma^i_j} & \mathbf{A}^{q_{vv}}_{\Gamma^i_j\Gamma^i_j} \end{bmatrix}^{-1} \begin{bmatrix} \mathbf{A}^{u_{ss}}_{\Gamma^i_j\Gamma^i_j} & \mathbf{A}^{u_{sv}}_{\Gamma^i_j\Gamma^i_j} \\ \mathbf{A}^{u_{vs}}_{\Gamma^i_j\Gamma^i_j} & \mathbf{A}^{u_{vv}}_{\Gamma^i_j\Gamma^i_j} \end{bmatrix}, \\ \begin{Bmatrix} \widehat{b}_{\Gamma^i_j} \\ \widehat{d}_{\Gamma^i_j} \end{Bmatrix} &= \begin{bmatrix} \mathbf{A}^{q_{ss}}_{\Gamma^i_j\Gamma^i_j} & \mathbf{A}^{q_{sv}}_{\Gamma^i_j\Gamma^i_j} \\ \mathbf{A}^{q_{vs}}_{\Gamma^i_j\Gamma^i_j} & \mathbf{A}^{q_{vv}}_{\Gamma^i_j\Gamma^i_j} \end{bmatrix}^{-1} \begin{Bmatrix} \overline{\mathbf{b}}_{\Gamma^i_j} \\ \overline{\mathbf{d}}_{\Gamma^i_j} \end{Bmatrix}, \end{aligned} \tag{34}$$

The same derivation processes can be repeated for the domain Ω_k ($k = 2 \cdots M$). The analog of Eq. (33) is given by

$$\begin{bmatrix} \widehat{A}^{u_{ss}}_{\Gamma^k_l\Gamma^k_l} & \widehat{A}^{u_{sv}}_{\Gamma^k_l\Gamma^k_l} \\ \widehat{A}^{u_{vs}}_{\Gamma^k_l\Gamma^k_l} & \widehat{A}^{u_{vv}}_{\Gamma^k_l\Gamma^k_l} \end{bmatrix} \begin{Bmatrix} \hat{\mathbf{u}}^s_{\Gamma^k_l} \\ \hat{\mathbf{u}}^v_{\Gamma^k_l} \end{Bmatrix} - \begin{Bmatrix} \hat{\mathbf{q}}^s_{\Gamma^k_l} \\ \hat{\mathbf{q}}^v_{\Gamma^k_l} \end{Bmatrix} = \begin{Bmatrix} \widehat{b}_{\Gamma^k_l} \\ \widehat{d}_{\Gamma^k_l} \end{Bmatrix}, \tag{35}$$

where l (l=1, 2, $\cdots$, M and $k \neq l$) is the index of subdomain contacting with the domain Ω_k.

3.2 Assembling the coefficient matrix for the interface

Additional conditions are required for unknown variables on the interface to couple adjacent subdomains. The point-element constraints on interface pair I^i_j-I^j_i are given by

$$\begin{aligned} u^s_{\Gamma^i_j} &= \mathbf{F}^{ss}_{\Gamma^i_j\Gamma^j_i} \mathbf{u}^s_{\Gamma^j_i} + \mathbf{F}^{sv}_{\Gamma^i_j\Gamma^j_i} \mathbf{u}^v_{\Gamma^j_i}, \\ u^v_{\Gamma^i_j} &= \mathbf{F}^{vs}_{\Gamma^i_j\Gamma^j_i} \mathbf{u}^s_{\Gamma^j_i} + \mathbf{F}^{vv}_{\Gamma^i_j\Gamma^j_i} \mathbf{u}^v_{\Gamma^j_i}, \end{aligned} \tag{36}$$

$$\begin{aligned} q^s_{\Gamma^j_i} &= -\mathbf{F}^{ss}_{\Gamma^j_i\Gamma^i_j} \mathbf{q}^s_{\Gamma^i_j} - \mathbf{F}^{sv}_{\Gamma^j_i\Gamma^i_j} \mathbf{q}^v_{\Gamma^i_j}, \\ q^v_{\Gamma^j_i} &= -\mathbf{F}^{vs}_{\Gamma^j_i\Gamma^i_j} \mathbf{q}^s_{\Gamma^i_j} - \mathbf{F}^{vv}_{\Gamma^j_i\Gamma^i_j} \mathbf{q}^v_{\Gamma^i_j}, \end{aligned} \tag{37}$$

where $\mathbf{F}^{ss}_{\Gamma_j^i\Gamma_i^j}$, $\mathbf{F}^{sv}_{\Gamma_j^i\Gamma_i^j}$, $\mathbf{F}^{vs}_{\Gamma_j^i\Gamma_i^j}$, and $\mathbf{F}^{vv}_{\Gamma_j^i\Gamma_i^j}$ are projection matrices from interface Γ_j^i to interface Γ_i^j. On the contrary, $\mathbf{F}^{ss}_{\Gamma_i^j\Gamma_j^i}$, $\mathbf{F}^{sv}_{\Gamma_i^j\Gamma_j^i}$, $\mathbf{F}^{vs}_{\Gamma_i^j\Gamma_j^i}$, and $\mathbf{F}^{vv}_{\Gamma_i^j\Gamma_j^i}$ are matrices from Γ_i^j to Γ_j^i. $\mathbf{u}^s_{\Gamma_i^j}$ and $\mathbf{u}^v_{\Gamma_i^j}$ are potential of the source and virtual nodes on dual interpolation element Γ_i^j. $\mathbf{q}^s_{\Gamma_j^i}$ and $\mathbf{q}^v_{\Gamma_j^i}$ are the flux on Γ_j^i.

Based on Eqs. (36), (37) the unknown flux in Eqs. (33), (35) can be condensed. Then a system of linear equations for the unknown potential on interfaces are given by

$$\begin{bmatrix} \mathbf{A}^{ss}_{\Gamma_j^i\Gamma_j^i} & \cdots & \mathbf{A}^{ss}_{\Gamma_j^i\Gamma_M^{M-1}} & \mathbf{A}^{sv}_{\Gamma_j^i\Gamma_j^i} & \cdots & \mathbf{A}^{sv}_{\Gamma_j^i\Gamma_M^{M-1}} \\ \vdots & & \vdots & \vdots & & \vdots \\ \mathbf{A}^{ss}_{\Gamma_M^{M-1}\Gamma_j^i} & \cdots & \mathbf{A}^{ss}_{\Gamma_M^{M-1}\Gamma_M^{M-1}} & \mathbf{A}^{sv}_{\Gamma_M^{M-1}\Gamma_2^1} & \cdots & \mathbf{A}^{sv}_{\Gamma_M^{M-1}\Gamma_M^{M-1}} \\ \mathbf{A}^{vs}_{\Gamma_j^i\Gamma_j^i} & \cdots & \mathbf{A}^{vs}_{\Gamma_j^i\Gamma_M^{M-1}} & \mathbf{A}^{vv}_{\Gamma_j^i\Gamma_j^i} & \cdots & \mathbf{A}^{vv}_{\Gamma_j^i\Gamma_M^{M-1}} \\ \vdots & & \vdots & \vdots & & \vdots \\ \mathbf{A}^{vs}_{\Gamma_M^{M-1}\Gamma_j^i} & \cdots & \mathbf{A}^{vs}_{\Gamma_M^{M-1}\Gamma_M^{M-1}} & \mathbf{A}^{vv}_{\Gamma_M^{M-1}\Gamma_j^i} & \cdots & \mathbf{A}^{vv}_{\Gamma_M^{M-1}\Gamma_M^{M-1}} \end{bmatrix} \begin{Bmatrix} \hat{\mathbf{u}}^s_{\Gamma_j^i} \\ \vdots \\ \hat{\mathbf{u}}^s_{\Gamma_M^{M-1}} \\ \hat{\mathbf{u}}^v_{\Gamma_j^i} \\ \vdots \\ \hat{\mathbf{u}}^v_{\Gamma_M^{M-1}} \end{Bmatrix} = \begin{Bmatrix} \hat{\mathbf{b}}_{\Gamma_j^i} \\ \vdots \\ \hat{\mathbf{b}}_{\Gamma_M^{M-1}} \\ \hat{\mathbf{d}}_{\Gamma_j^i} \\ \vdots \\ \hat{\mathbf{d}}_{\Gamma_M^{M-1}} \end{Bmatrix}, \tag{38}$$

where

$$\begin{Bmatrix} \hat{\mathbf{b}}_{\Gamma_j^i} \\ \vdots \\ \hat{\mathbf{b}}_{\Gamma_M^{M-1}} \\ \hat{\mathbf{d}}_{\Gamma_j^i} \\ \vdots \\ \hat{\mathbf{d}}_{\Gamma_M^{M-1}} \end{Bmatrix} = \begin{Bmatrix} \widehat{b}_{\Gamma_j^i} + \mathbf{F}^{ss}_{\Gamma_j^i\Gamma_i^j}\widehat{b}_{\Gamma_i^j} + \mathbf{F}^{sv}_{\Gamma_j^i\Gamma_i^j}\widehat{d}_{\Gamma_i^j} \\ \vdots \\ \widehat{b}_{\Gamma_M^{M-1}} + \mathbf{F}^{ss}_{\Gamma_M^{M-1}\Gamma_{M-1}^M}\widehat{b}_{\Gamma_{M-1}^M} + \mathbf{F}^{sv}_{\Gamma_M^{M-1}\Gamma_{M-1}^M}\widehat{d}_{\Gamma_{M-1}^M} \\ \widehat{d}_{\Gamma_j^i} + \mathbf{F}^{ss}_{\Gamma_j^i\Gamma_i^j}\widehat{b}_{\Gamma_i^j} + \mathbf{F}^{sv}_{\Gamma_j^i\Gamma_i^j}\widehat{d}_{\Gamma_i^j} \\ \vdots \\ \widehat{d}_{\Gamma_M^{M-1}} + \mathbf{F}^{ss}_{\Gamma_M^{M-1}\Gamma_{M-1}^M}\widehat{b}_{\Gamma_{M-1}^M} + \mathbf{F}^{sv}_{\Gamma_M^{M-1}\Gamma_{M-1}^M}\widehat{d}_{\Gamma_{M-1}^M} \end{Bmatrix}. \tag{39}$$

Hereafter, the symbol M_i denotes the master interface (i.e. Γ_j^i, $(i < j)$) in the domain Ω_i, and S_j denotes the slave interface (i.e. Γ_i^j, $(i < j)$) in Ω_j. The assembly rules of the interface coefficient matrix abide by

rule1: when Ω_i=Ω_j and M_i=M_j

$$\mathbf{A}^{ss}_{M_iM_j} = {}^i\widehat{A}^{ss}_{M_iM_j} + \mathbf{F}^{ss}_{M_iS_i}{}^j\widehat{A}^{ss}_{S_iS_j}\mathbf{F}^{ss}_{S_jM_j} + \mathbf{F}^{ss}_{M_iS_i}{}^j\widehat{A}^{sv}_{S_iS_j}\mathbf{F}^{vs}_{S_jM_j} + \mathbf{F}^{sv}_{M_iS_i}{}^j\widehat{A}^{vs}_{S_iS_j}\mathbf{F}^{ss}_{S_jM_j} + \mathbf{F}^{sv}_{M_iS_i}{}^j\widehat{A}^{vv}_{S_iS_j}\mathbf{F}^{vs}_{S_jM_j}, \tag{40}$$

$$\mathbf{A}^{sv}_{M_iM_j} = {}^i\widehat{A}^{sv}_{M_iM_j} + \mathbf{F}^{ss}_{M_iS_i}{}^j\widehat{A}^{ss}_{S_iS_j}\mathbf{F}^{sv}_{S_jM_j} + \mathbf{F}^{ss}_{M_iS_i}{}^j\widehat{A}^{sv}_{S_iS_j}\mathbf{F}^{vv}_{S_jM_j} + \mathbf{F}^{sv}_{M_iS_i}{}^j\widehat{A}^{vs}_{S_iS_j}\mathbf{F}^{sv}_{S_jM_j} + \mathbf{F}^{sv}_{M_iS_i}{}^j\widehat{A}^{vv}_{S_iS_j}\mathbf{F}^{vv}_{S_jM_j}, \tag{41}$$

$$\mathbf{A}^{vs}_{M_iM_j} = {}^i\widehat{A}^{vs}_{M_iM_j} + \mathbf{F}^{vs}_{M_iS_i}{}^j\widehat{A}^{ss}_{S_iS_j}\mathbf{F}^{ss}_{S_jM_j} + \mathbf{F}^{vs}_{M_iS_i}{}^j\widehat{A}^{sv}_{S_iS_j}\mathbf{F}^{vs}_{S_jM_j} + \mathbf{F}^{vv}_{M_iS_i}{}^j\widehat{A}^{vs}_{S_iS_j}\mathbf{F}^{ss}_{S_jM_j} + \mathbf{F}^{vv}_{M_iS_i}{}^j\widehat{A}^{vv}_{S_iS_j}\mathbf{F}^{vs}_{S_jM_j}, \tag{42}$$

$$\mathbf{A}^{vv}_{M_iM_j} = {}^i\widehat{A}^{vv}_{M_iM_j} + \mathbf{F}^{vs}_{M_iS_i}{}^j\widehat{A}^{ss}_{S_iS_j}\mathbf{F}^{sv}_{S_jM_j} + \mathbf{F}^{vs}_{M_iS_i}{}^j\widehat{A}^{sv}_{S_iS_j}\mathbf{F}^{vv}_{S_jM_j} + \mathbf{F}^{vv}_{M_iS_i}{}^j\widehat{A}^{vs}_{S_iS_j}\mathbf{F}^{sv}_{S_jM_j} + \mathbf{F}^{vv}_{M_iS_i}{}^j\widehat{A}^{vv}_{S_iS_j}\mathbf{F}^{vv}_{S_jM_j}; \tag{43}$$

rule2: when $\Omega_i \neq \Omega_j$.

(i) M_i, M_j belong to the same subdomain:

$$\mathbf{A}^{ss}_{M_iM_j} = {}^i\widehat{A}^{ss}_{M_iM_j}, \tag{44}$$

$$\mathbf{A}^{sv}_{M_iM_j} = {}^i\widehat{A}^{sv}_{M_iM_j}, \tag{45}$$

$$\mathbf{A}^{vs}_{M_iM_j} = {}^i\widehat{A}^{vs}_{M_iM_j}, \tag{46}$$

$$\mathbf{A}^{vv}_{M_iM_j} = {}^i\widehat{A}^{vv}_{M_iM_j}. \tag{47}$$

(ii) M_i, S_j belong to the same subdomain

$$\mathbf{A}^{ss}_{M_iM_j} = {}^{i}\widehat{A}^{ss}_{M_iS_j}\mathbf{F}^{ss}_{S_jM_j} + {}^{i}\widehat{A}^{sv}_{M_iS_j}\mathbf{F}^{vs}_{S_jM_j}, \tag{48}$$

$$\mathbf{A}^{sv}_{M_iM_j} = {}^{i}\widehat{A}^{ss}_{M_iS_j}\mathbf{F}^{sv}_{S_jM_j} + {}^{i}\widehat{A}^{sv}_{M_iS_j}\mathbf{F}^{vv}_{S_jM_j}, \tag{49}$$

$$\mathbf{A}^{vs}_{M_iM_j} = {}^{i}\widehat{A}^{vs}_{M_iS_j}\mathbf{F}^{ss}_{S_jM_j} + {}^{i}\widehat{A}^{vv}_{M_iS_j}\mathbf{F}^{vs}_{S_jM_j}, \tag{50}$$

$$\mathbf{A}^{vv}_{M_iM_j} = {}^{i}\widehat{A}^{vs}_{M_iS_j}\mathbf{F}^{sv}_{S_jM_j} + {}^{i}\widehat{A}^{vv}_{M_iS_j}\mathbf{F}^{vv}_{S_jM_j}. \tag{51}$$

(iii) S_i, M_j belong to the same subdomain:

$$\mathbf{A}^{ss}_{M_iM_j} = \mathbf{F}^{ss}_{M_iS_i}{}^{j}\widehat{A}^{ss}_{S_iM_j} + \mathbf{F}^{sv}_{M_iS_i}{}^{j}\widehat{A}^{vs}_{S_iM_j}, \tag{52}$$

$$\mathbf{A}^{sv}_{M_iM_j} = \mathbf{F}^{ss}_{M_iS_i}{}^{j}\widehat{A}^{sv}_{S_iM_j} + \mathbf{F}^{sv}_{M_iS_i}{}^{j}\widehat{A}^{vv}_{S_iM_j}, \tag{53}$$

$$\mathbf{A}^{vs}_{M_iM_j} = \mathbf{F}^{vs}_{M_iS_i}{}^{j}\widehat{A}^{ss}_{S_iM_j} + \mathbf{F}^{vv}_{M_iS_i}{}^{j}\widehat{A}^{vs}_{S_iM_j}, \tag{54}$$

$$\mathbf{A}^{vv}_{M_iM_j} = \mathbf{F}^{vs}_{M_iS_i}{}^{j}\widehat{A}^{sv}_{S_iM_j} + \mathbf{F}^{vv}_{M_iS_i}{}^{j}\widehat{A}^{vv}_{S_iM_j}. \tag{55}$$

(iv) S_i, S_j belong to the same subdomain:

$$\mathbf{A}^{ss}_{M_iM_j} = \mathbf{F}^{ss}_{M_iS_i}{}^{j}\widehat{A}^{ss}_{S_iS_j}\mathbf{F}^{ss}_{S_jM_j} + \mathbf{F}^{ss}_{M_iS_i}{}^{j}\widehat{A}^{sv}_{S_iS_j}\mathbf{F}^{vs}_{S_jM_j} + \mathbf{F}^{sv}_{M_iS_i}{}^{j}\widehat{A}^{vs}_{S_iS_j}\mathbf{F}^{ss}_{S_jM_j} + \mathbf{F}^{sv}_{M_iS_i}{}^{j}\widehat{A}^{vv}_{S_iS_j}\mathbf{F}^{vs}_{S_jM_j}, \tag{56}$$

$$\mathbf{A}^{sv}_{M_iM_j} = \mathbf{F}^{ss}_{M_iS_i}{}^{j}\widehat{A}^{ss}_{S_iS_j}\mathbf{F}^{sv}_{S_jM_j} + \mathbf{F}^{ss}_{M_iS_i}{}^{j}\widehat{A}^{sv}_{S_iS_j}\mathbf{F}^{vv}_{S_jM_j} + \mathbf{F}^{sv}_{M_iS_i}{}^{j}\widehat{A}^{vs}_{S_iS_j}\mathbf{F}^{sv}_{S_jM_j} + \mathbf{F}^{sv}_{M_iS_i}{}^{j}\widehat{A}^{vv}_{S_iS_j}\mathbf{F}^{vv}_{S_jM_j}, \tag{57}$$

$$\mathbf{A}^{vs}_{M_iM_j} = \mathbf{F}^{vs}_{M_iS_i}{}^{j}\widehat{A}^{ss}_{S_iS_j}\mathbf{F}^{ss}_{S_jM_j} + \mathbf{F}^{vs}_{M_iS_i}{}^{j}\widehat{A}^{sv}_{S_iS_j}\mathbf{F}^{vs}_{S_jM_j} + \mathbf{F}^{vv}_{M_iS_i}{}^{j}\widehat{A}^{vs}_{S_iS_j}\mathbf{F}^{ss}_{S_jM_j} + \mathbf{F}^{vv}_{M_iS_i}{}^{j}\widehat{A}^{vv}_{S_iS_j}\mathbf{F}^{vs}_{S_jM_j}, \tag{58}$$

$$\mathbf{A}^{vv}_{M_iM_j} = \mathbf{F}^{vs}_{M_iS_i}{}^{j}\widehat{A}^{ss}_{S_iS_j}\mathbf{F}^{sv}_{S_jM_j} + \mathbf{F}^{vs}_{M_iS_i}{}^{j}\widehat{A}^{sv}_{S_iS_j}\mathbf{F}^{vv}_{S_jM_j} + \mathbf{F}^{vv}_{M_iS_i}{}^{j}\widehat{A}^{vs}_{S_iS_j}\mathbf{F}^{sv}_{S_jM_j} + \mathbf{F}^{vv}_{M_iS_i}{}^{j}\widehat{A}^{vv}_{S_iS_j}\mathbf{F}^{vv}_{S_jM_j}. \tag{59}$$

If there are no interfaces between two subdomains, the relevant block is **0** in the interface coefficient matrix, and the sparsity is more and more significant with the increasing number of subdomains.

4 Numerical examples

The accuracy and convergence of the proposed method in the 3D steady-state heat conduction problem will be demonstrated by the analytical solution problem next part. Then, two real-life examples with thin structures will be employed to illustrate the computational efficiency and excellent performance. Error estimation of the presented method is measured by the relative error, defined by

$$\text{error} = \frac{1}{\left|v^{(e)}\right|_{\max}}\sqrt{\frac{1}{M}\sum_{i=1}^{M}[v_i^{(e)} - v_i^{(n)}]^2}, \tag{60}$$

where $\left|v^{(e)}\right|_{\max}$ is the maximum value of the exact temperature u or flux q over M sample points, and superscripts e and n denote the exact and numerical solutions, respectively.

The following examples, unless otherwise mentioned, $\overline{q}$ and $\overline{u}$ represent the prescribed flux and temperature conditions. "Err_q", "NE" and "NS" denote the relative errors for flux, the number of elements, and source points, respectively.

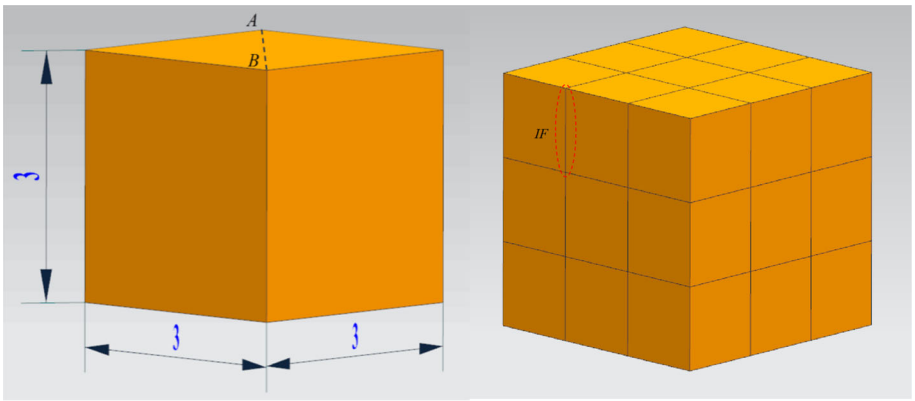

Fig. 4 Model for cube **a** single-domain **b** multi-domain

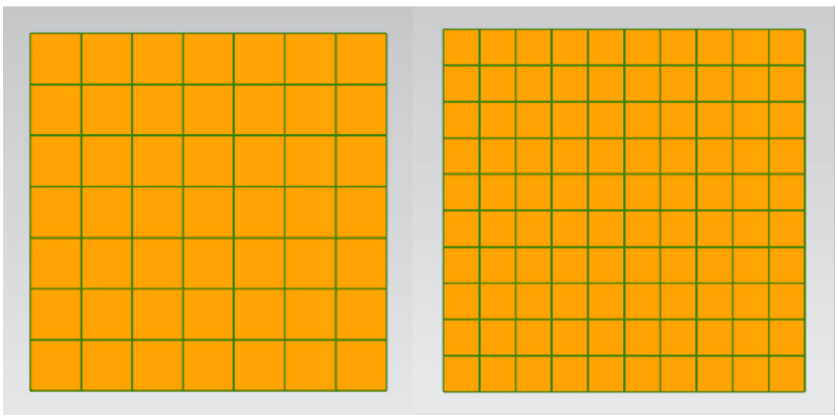

Fig. 5 Mesh assignment along interface *IF*

4.1 Cube

In order to examine the capability of the proposed multi-domain method in dealing with the case when one subdomain is surrounded by others, a cube with 27 subdomains (see Fig. 4b) is employed in a quadratic potential field problem, and geometric dimension is shown in Fig. 4a. Dirichlet boundary conditions (see Eq. (61) are imposed on all boundary faces, and the analytical solution is given by:

$$U = -2x_1^2 + x_2^2 + x_3^2. \tag{61}$$

In this example, a free mesh scheme is adopted between interfaces to verify the ability of the node-to-element mapping method (see Fig. 5). The dual interpolation constant element in DiBFM is used to discretize BIE. Continuous and isotropic material is assumed uniformly, and heat conductivity coefficient is taken as $k = 1.0$ W/(m.K).

The relative errors of normal flux are listed in Table 1, this table demonstrates that the accuracy of our multi-domain method improves gradually with the increasing number of source points, and the convergence can be illustrated as well. The graphic in Fig. 6 compares the normal flux along with line AB, which indicates that both numerical results of single-domain DiBFM (with 7938 source nodes) and multi-domain DiBFM (with 7776 source nodes) have a good agreement with the exact solution. The contour plots in Figs. 7a, c describe the experimental result for the normal flux calculated by two algorithms. Figure 7b depicts the distribution of the normal flux on the interfaces obtained by the presented multi-domain algorithm.

The numerical results presented above have sufficiently illustrated our algorithm's reliability and capability.

Table 1 Relative error for flux between single-domain method and multi-domain method

Multi-domain DiBFM			Single-domain DiBFM		
NE	NS	Err_Flux	NE	NS	Err_Flux
648	648	5.30E−07	600	600	4.22E−07
2927	2927	8.24E−08	2646	2646	7.41E−08
4050	4050	6.56E−08	4056	4056	4.59E−08
7938	7938	2.32E−08	7776	7776	1.83E−08

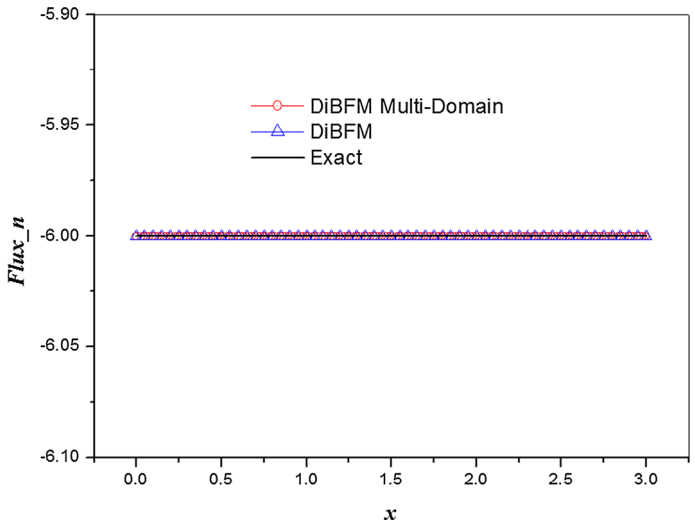

Fig. 6 Comparison of the normal flux along with line AB

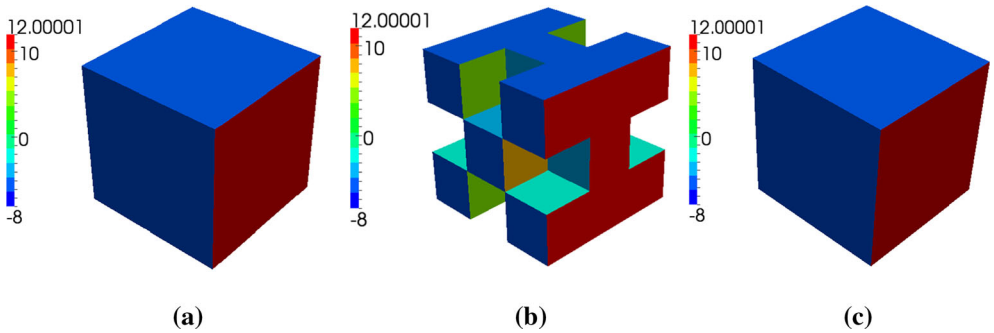

Fig. 7 Numerical result for normal flux **a** multi-domain DiBFM with 7938 source nodes, **b** part of multi-domain and **c** single-domain DiBFM with 7776 source nodes

4.2 Cellular structure

To study the accuracy and convergence of our multi-domain method in handling problems with small feature sizes, let us consider a cellular structure with a thin wall that is subdivided into 7 subdomains (see Fig. 8b). Relative parameters are shown in Fig. 8a. The employment of a cubic polynomial solution is to illustrate the validity of the proposed method in the high-order analytical field problem.

Dirichlet boundary conditions are prescribed on the outer surfaces. All subdomains are continuous and isotropic, and heat conductivity coefficient $k = 1.0$ W/(m.K) is considered. Different meshes are assigned on interface pairs (see Fig. 9). The physical variables are approximated by the dual interpolation constant elements. The cubic polynomial solution is given by:

$$U = x_1^3 + x_2^3 + x_3^3 - 3(x_1^2 x_2 + x_2^2 x_3 + x_1 x_3^2). \tag{62}$$

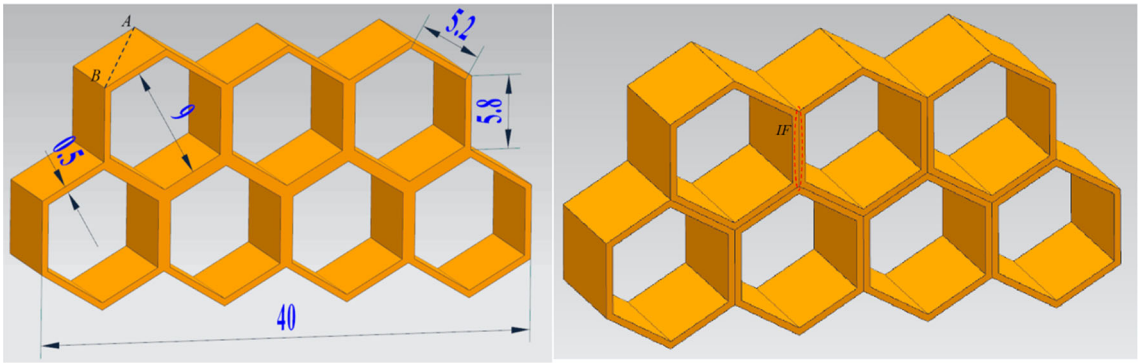

(a) **(b)**

Fig. 8 Model for cellular structure **a** single-domain **b** multi-domain

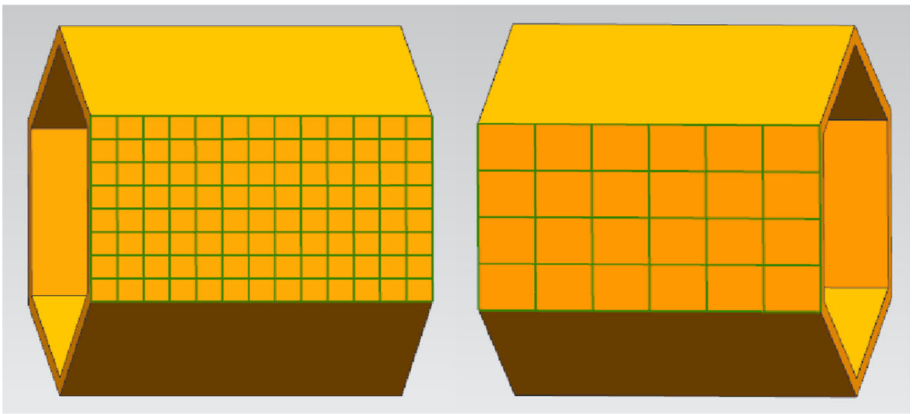

Fig. 9 Mesh assignment along interface *IF*

Table 2 Relative error for flux between single-domain method and multi-domain method

Multi-domain DiBFM			Single-domain DiBFM		
NE	NS	Err_Flux	NE	NS	Err_Flux
2772	2772	5.74E−03	2538	2538	3.55E−03
4158	4158	9.06E−04	4110	4110	7.92E−04
6972	6972	2.63E−04	6424	6424	1.89E−04
9450	9450	7.79E−05	9090	9090	6.19E−05

The variation of the relative errors on normal flux with the increasing number of the elements is listed in Table 2, which denotes numerical results by two methods tend to exact solution gradually. On the other hand, the convergence of the current method can be verified. In Fig. 10, the numerical results of the normal flux along with the line AB by the single-domain DiBFM (using 9450 source points) and multi-domain DiBFM (using 9090 source points) are compared with the exact solution, respectively. The contour plots of the normal flux by two algorithms are demonstrated in Figs. 11a–c.

These results above indicates that the present method guarantees an accurate simulation of the higher-order analytical field problem in geometric structures with thin walls and demonstrate the convergence of the proposed multi-domain approach.

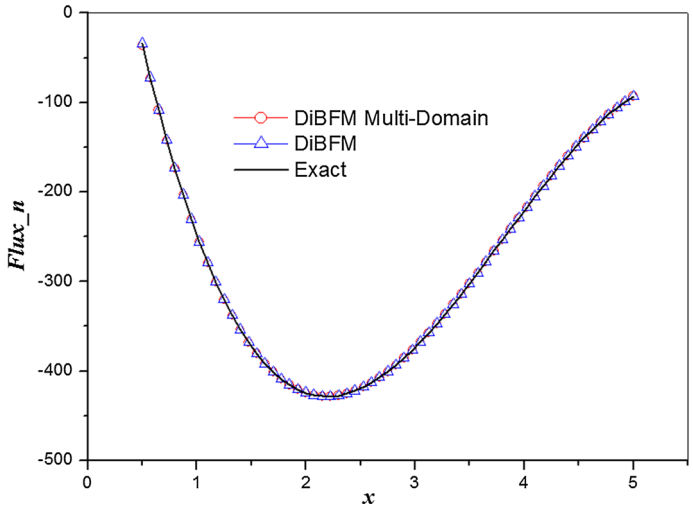

Fig. 10 Comparison of the normal flux along with line AB

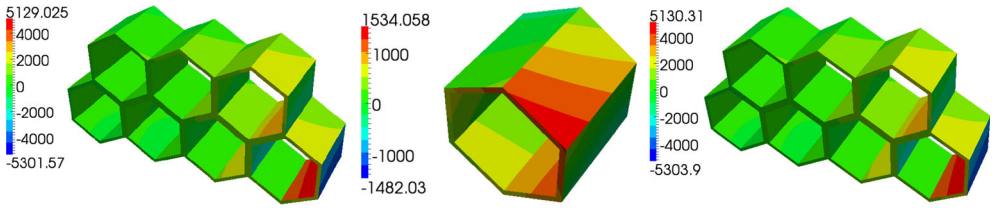

Fig. 11 Numerical result for normal flux **a** multi-domain DiBFM with 9450 source nodes, **b** part of multi-domain and **c** single-domain DiBFM with 9090 source nodes

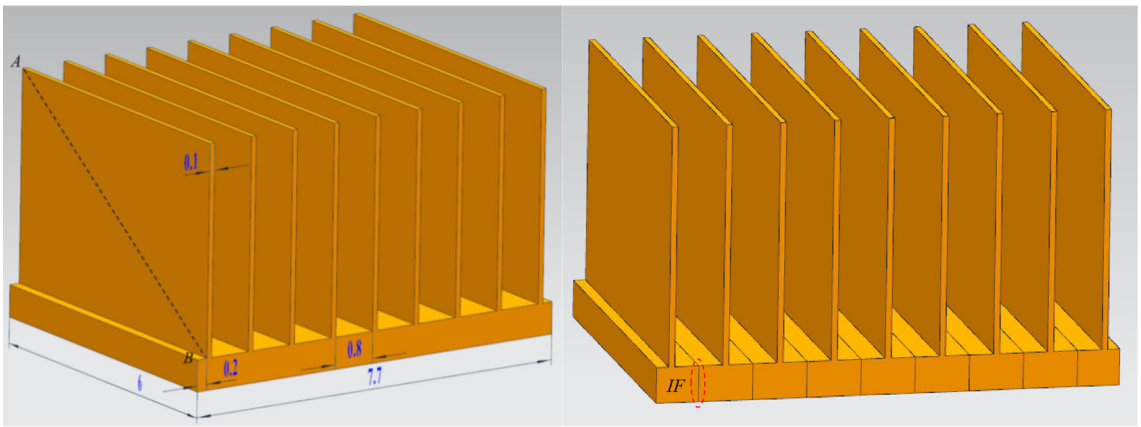

Fig. 12 Model for heat radiator **a** single-domain **b** multi-domain

4.3 Heat radiator

To test the practicability of the present method in coping with real-life problems, the following example concerns a heat radiator divided into 9 subdomains, as shown in Fig. 12b. The size of this thin structure is dimensioned in Fig. 12a.

Homogeneous and isotropic characters are considered in this example. The bottom surface is subject to a steady temperature $T = 100$ K, and the remaining surfaces are confined to flux boundary condition $q = 0.1$ W/m^2. Heat conductivity coefficient is $k = 20$ W/ (m.K). As mentioned in the above examples, the same

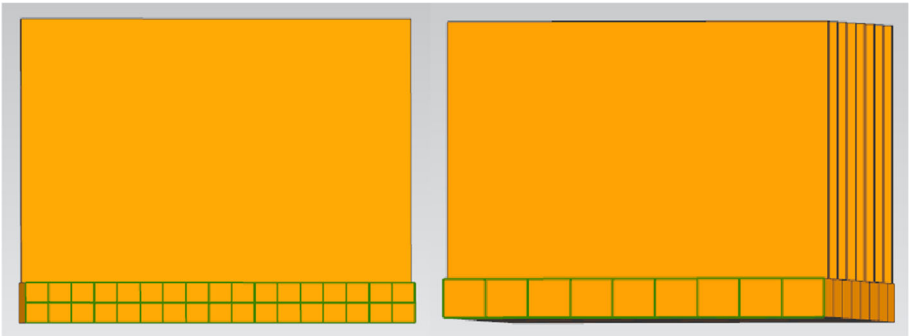

Fig. 13 Mesh assignment along interface *IF*

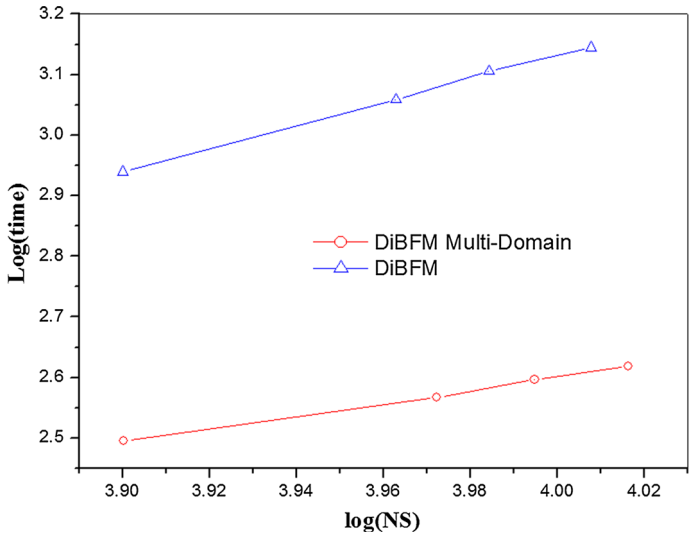

Fig. 14 Comparison of efficiency between multi-domain DiBFM and single-domain DiBFM

mesh-division scheme is performed on the interface groups, as shown in Fig. 13. The physical variables are approximated by the dual interpolation constant elements, while quadratic elements in FEM.

The comparison of the computational efficiency between single-domain DiBFM and multi-domain DiBFM is shown in Fig. 14. Where the x-coordinate is the log of the number of source points, and y-coordinate is the log of the CPU time. This figure shows that less CPU time is consumed in the multi-domain method under similar source points. Figure 15 describes the temperature along with line AB by multi-domain DiBFM with 9546 source nodes, single-domain DiBFM with 9108 source nodes, and FEM with 165,383 nodes. The results of these methods are almost identical, and the reliability of the proposed method can be confirmed.

Contour plots in Fig. 16 present the temperature distribution calculated by different algorithms, from which we can note that the steady-state of the thermal by our method has little difference with DiBFM and FEM, but the interface results outlined in Fig. 16b testified the reliability of by our algorithm.

The information above illustrates the practicability and validity of our method in dealing with thin structures with a real engineering background.

4.4 Fuel cell structure

In the last example, we perform the numerical experiment in a fuel cell structure to investigate the feasibility and performance of our algorithms in a more complex case. The dimension of the geometric model is shown in Fig. 17a, and the multi-domain model with 9 subdomains is shown in Fig. 17b.

Assuming that, the material is homogeneous and isotropic. Environment temperature is $U = 22$ K, and temperature boundary condition $T = 100$ K is imposed on the inner surface of the cylinder. The convection

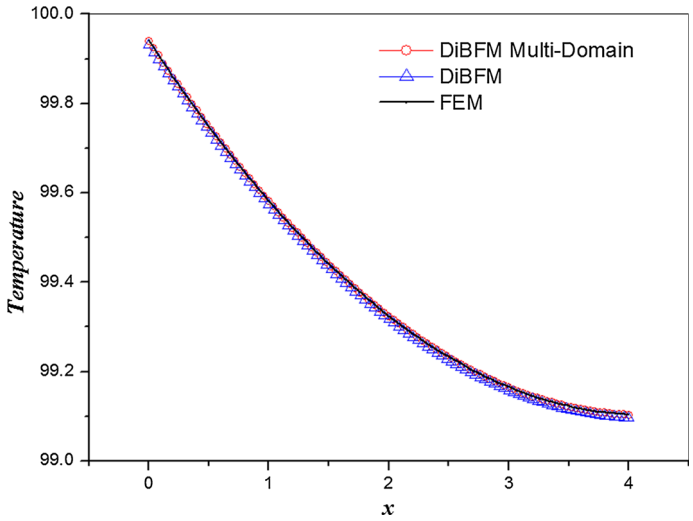

Fig. 15 Comparison of temperature along line AB

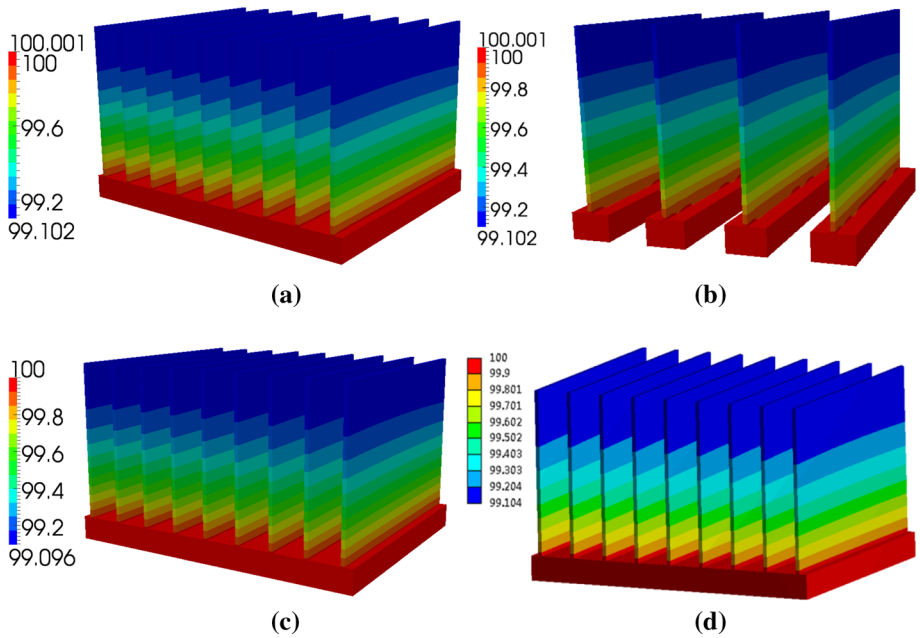

Fig. 16 Numerical result for temperature **a** multi-domain DiBFM with 9546 source nodes, **b** part of multi-domain, **c** single-domain DiBFM with 9108 source nodes, and **d** FEM with 165,383 nodes

boundary condition is prescribed on remanent surfaces. Heat conductivity coefficient $k = 90.6$ W/ (m.K) and convection coefficient λ=0.2 W/ (m^2.K) is selected. The assignment of meshes between interface pairs is shown in Fig. 18. The physical variables are approximated by the dual interpolation constant elements and by quadratic elements in FEM.

Four groups are listed in Fig. 19 for comparative purposes in computational efficiency between single-domain DiBFM and multi-domain DiBFM. Where the x-coordinate is the log of the number of source points, and y-coordinate is the log of the CPU time. This figure can draw the same conclusion as Sect. 4.3: the multi-domain method has higher computational efficiency than the single one when comparable source points are adopted. Figure 20 gives the temperature along with line AB by multi-domain DiBFM with 9087 source nodes, single-domain DiBFM with 8966 source nodes, and FEM with 225,638 nodes. The discrepancies between our method and FEM are within the range of error. Thus, the reliability of the proposed method can be verified.

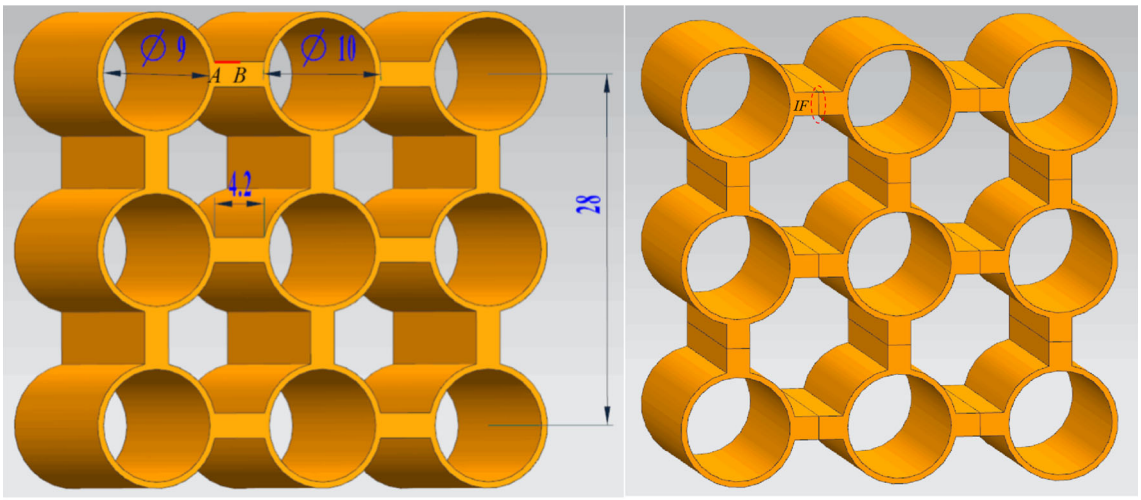

Fig. 17 Model for fuel cell structure **a** single-domain **b** multi-domain

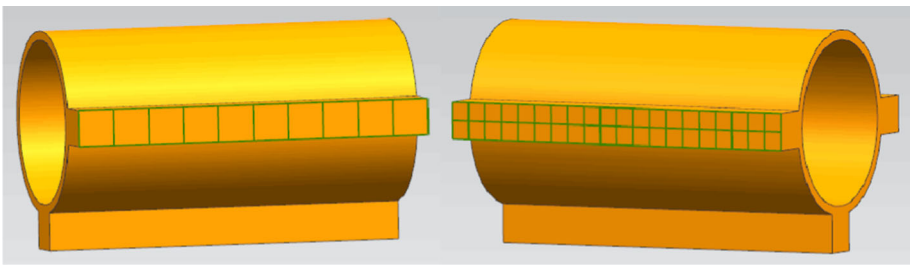

Fig. 18 Mesh assignment along interface *IF*

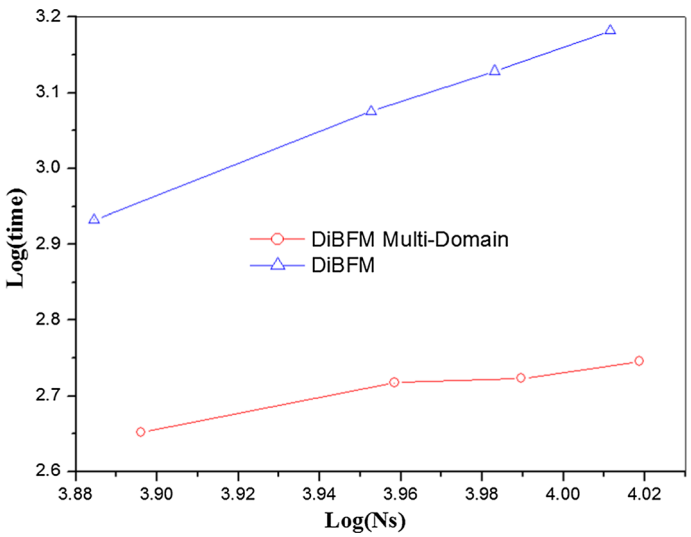

Fig. 19 Comparison of efficiency between multi-domain DiBFM and single-domain DiBFM

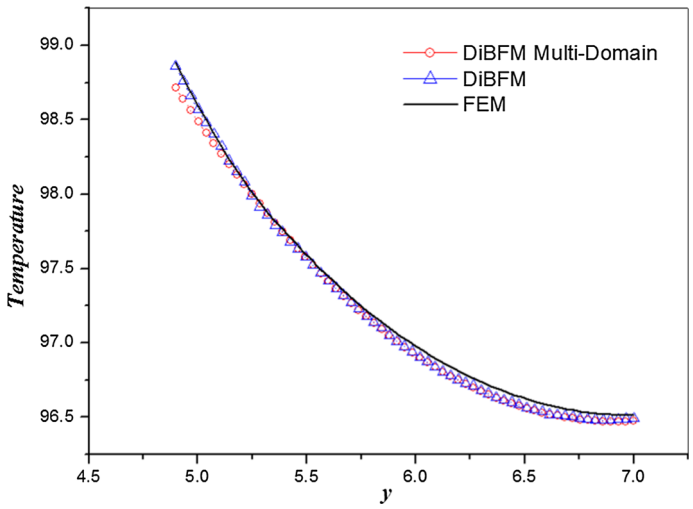

Fig. 20 Comparison of temperature along with line AB

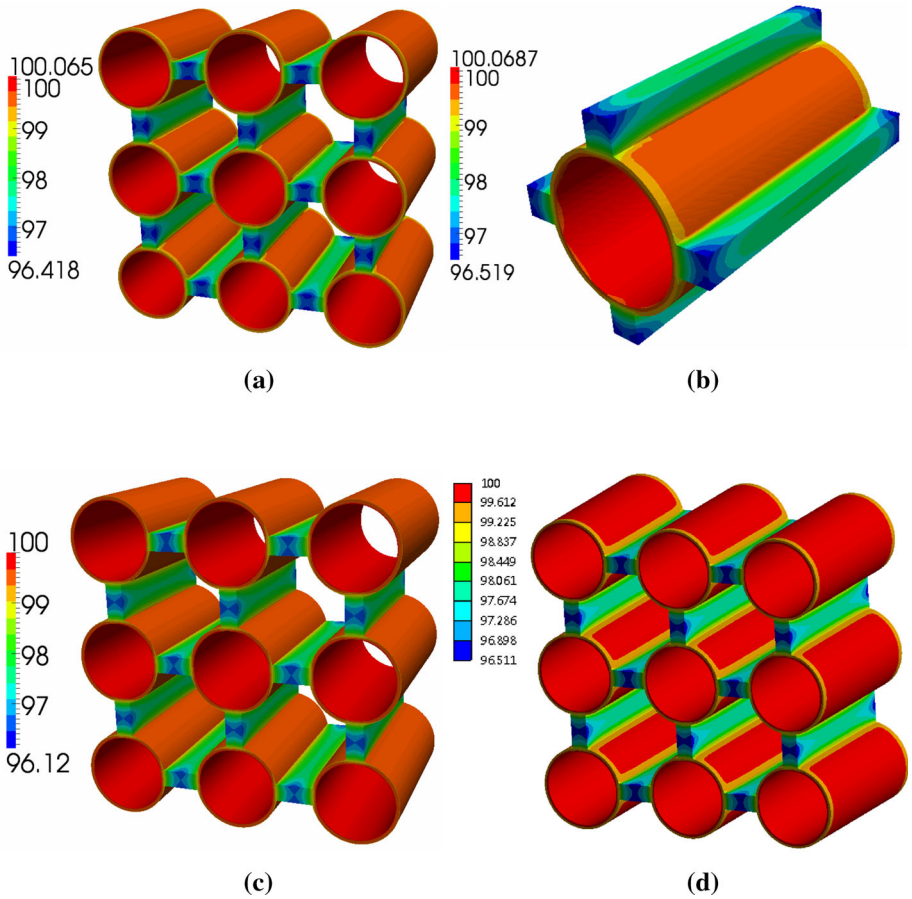

Fig. 21 Numerical result for temperature **a** multi-domain DiBFM with 9087source nodes, **b** part of multi-domain, **c** single-domain DiBFM with 8966 source nodes, and **d** FEM with 225,638 nodes

Figures 21a–d present the contour plots of the temperature obtained by those algorithms mentioned above. The max value of the temperature by our method is just 0.065% higher than the reference methods. The contour plot for one of the subdomains is plotted in Fig. 21b to view the temperature on the interface.

This demonstrates that our method feasible in solving more complicated structures with a thin feature, and the excellent performance of the proposed method is also shown.

5 Conclusions and discussions

In this paper, a multi-domain method based on DiBFM-HMLS has been proposed, and the condensation technology was employed to get the system of linear equations only concerning unknown interfacial variables. For different subdomains, the assembly rules to form the overall coefficient matrix have been elaborated on in this article. Compared with the single-domain DiBFM-HMLS, the multi-domain DiBFM-HMLS takes less CPU time when solving complex geometric structures. A point-to-element interpolation relationship has been constructed based on the dual interpolation element instead of a conventional node-to-node one. The introduction of DiBFM-HMLS guarantees an accurate interpolation for corner points and lets the multi-domain method has superiority in dealing with structures with a thin or small feature, as reflected in the numerical experiments. Simultaneously, the reliability and convergence of the presented method have been illustrated by those examples.

Since the meshes could be discontinuous and the integral in BIE can be calculated separately; thus parallelization can be performed on these parts. According to the hierarchical matrix theory and low-rank approximation theory, the far-field block of the coefficient matrix can be approximated by low-rank matrix, and this can save the memory and provide the possibility for solving the large-scale problem using multi-domain DiBFM. The addressed method was only applied to analyze thermal conduction problems ordinarily. In future work, this method will be used to solve elastodynamic problems, dynamic contact problems, and large-scale problems by supplementing the fast algorithm; the goal will come true soon. The demonstrated method is in progress for the 3D elastostatic multi-domain problem.

Acknowledgements This work was supported by National Natural Science Foundation of China under grant numbers 11772125 and 11972010.

References

1. Zhang, J.M.: Multidomain thermal simulation of CNT composites by hybrid BNM. Numer. Heat Transf. Part B Fundam. **53**(3), 246–258 (2008)
2. Davì, G., Milazzo, A.: Multidomain boundary integral formulation for piezoelectric materials fracture mechanics. Int. J. Solids Struct. **38**(40–41), 7065–7078 (2001)
3. Ahmad, S., Banerjee, P.K.: Multi-domain BEM for two-dimensional problems of elastodynamics. Int. J. Numer. Meth. Eng. **26**(4), 891–911 (1988)
4. Kane, J.H.: Boundary Element Analysis in Engineering Continuum Mechanics. Prentice Hall, Englewood Cliffs (1994)
5. Layton, J.B., Guanguly, S., Balakrishna, C., Kane, J.H.: A symmetric Galerkin multi-zone boundary element formulation. Int. J. Numer. Methods Eng. **40**(16), 2913–2931 (1997)
6. Kallivokas, L.F., Juneja, T., Bielak, J.: A symmetric Galerkin BEM variational framework for multi-domain interface problems. Comput. Methods Appl. Mech. Eng. **194**(34–35), 3607–3636 (2005)
7. Chen, T.Z., Wang, B., Gen, Z.Z., Wu, Z.S.: A symmetric Galerkin multi-zone boundary element method for cohesive crack growth. Eng. Fract. Mech. **63**(5), 591–609 (1999)
8. Ramšak, M., Škerget, L., Hriberšek, M., Žunič, Z.: A multidomain boundary element method for unsteady laminar flow using stream function-vorticity equations. Eng. Anal. Bound. Elem. **29**(1), 1–14 (2005)
9. Baumann, M., van Gijzen, M.B.: Convergence and complexity study of GMRES variants for solving multi-frequency elastic wave propagation problems. J. Comput. Sci. **26**, 285–293 (2018)
10. Zhang, J.M., Zhuang, C., Qin, X.Y., Li, G.Y., Sheng, X.M.: FMM-accelerated hybrid boundary node method for multi-domain problems. Eng. Anal. Bound. Elem. **34**(5), 433–439 (2010)
11. Chaillat, S., Bonnet, M., Semblat, J.F.: A new fast multi-domain BEM to model seismic wave propagation and amplification in 3-D geological structures. Geophys. J. Int. **177**(2), 509–531 (2009)
12. Huang, S., Liu, Y.J.: A new simple multidomain fast multipole boundary element method. Comput. Mech. **58**(3), 533–548 (2016)
13. Liang, Y., Gao, X.W., Xu, B.B., Zhu, Q.H., Wu, Z.Y.: A new alternating iteration strategy based on the proper orthogonal decomposition for solving large-scaled transient nonlinear heat conduction problems. J. Comput. Sci. **45**, 101206 (2020)
14. Peng, H.F., Bai, Y.G., Yamg, K., Gao, X.W.: Three-step multi-domain BEM for solving transient multi-media heat conduction problems. Eng. Anal. Bound. Elem. **37**(11), 1545–1555 (2013)

15. Zheng, Y.T., Gao, X.W., Peng, H.F., Xu, B.B.: The coupled method of multi-domain BEM and element differential method for solving multi-scale problems. Eng. Anal. Bound. Elem. **113**, 145–155 (2020)
16. Gao, X.W., Guo, L., Zhang, C.: Three-step multi-domain BEM solver for nonhomogeneous material problems. Eng. Anal. Bound. Elem. **31**(12), 965–973 (2007)
17. Zhang, J.M., Lin, W.C., Dong, Y.Q., Ju, C.M.: A double-layer interpolation method for BIE implementation for potential problems. Appl. Math. Model. **51**, 250–269 (2017)
18. Zhang, J.M., Lin, W.C., Dong, Y.Q.: A dual interpolation boundary face method for elasticity problems. Eur. J. Mech. A Solids **73**, 500–511 (2019)
19. Zhang, J.M., Chi, B.T., Lin, W.C., Ju, C.M.: A dual interpolation boundary face method for three-dimensional potential problems. Int. J. Heat Mass Transf. **140**, 862–876 (2019)
20. Zhang, J.M., He, R., Chi, B.T., Lin, W.C.: A dual interpolation boundary face method with Hermite-type approximation for potential problems. Appl. Math. Model. **81**, 457–472 (2020)
21. Zhang, J.M., He, R., Lin, W.C., Yang, L., Chi, B.T., Ju, C.M.: A dual interpolation boundary face method with Hermite-type approximation for elasticity problems. Eur. J. Mech. A Solids **82**, 104005 (2020)
22. Liu, Y.: Fast Multipole Boundary Element Method: Theory and Applications in Engineering. Cambridge University Press, Cambridge (2009)
23. Xie, G., Wang, L., Zhang, J., et al.: Calculation of three-dimensional nearly singular boundary element integrals for steady-state heat conduction. Eng. Anal. Bound. Elem. **60**, 137–143 (2015)
24. Xie, G., Zhou, F., Zhong, Y., Geng, H., Wu, C.: Bi-directional sinh transformations based on the generalized Duffy space for nearly singular integrals. J. Comput. Appl. Math. **380**, 112981 (2020)